Flow field and phase distribution inside effervescent atomizers

Marc Lörcher[1]**, Florian Schmidt**[2] **and Dieter Mewes**[2]
1. Bayer AG, BTS-ENG-CP-ACSC, Rheinufer 7-9, R85, 47829 Krefeld
2. University of Hannover, Institut für Verfahrenstechnik (Process Engineering), Callinstr. 36, 30167 Hannover, Germany
e-mail: dms@ifv.uni-hannover.de

Abstract
Liquids or suspensions are dispersed into sprays of small droplets by atomization of two-phase gas-liquid mixtures. In this manner narrow droplet diameter distributions or large interfaces of the liquid phase are generated in order to increase heat- and mass-transfer. The mean droplet diameter of the spray is time dependent. It also depends on the total pressure upstream of the nozzle, the volumetric flow rate of the liquid and the gas phase, as well as on the flow regime inside the nozzle. The radial and axial profiles of the void fraction inside the nozzle are measured with an electrical measurement technique. In addition, the flow in the nozzle is visualized by a high-speed camera. Three flow regimes are identified. A model is established to predict the flow regime inside the atomizer. It turned out that the flow regime changes by accelerating the flow to critical conditions. The visualized flow fields are compared with calculated ones.

Nomenclature

d	$[m]$	diameter	e	$[-]$	energy ratio
g	$[-]$	statistical expression of the asymmetry	h	$[-]$	probability density function
j	$[\frac{m}{s}]$	superficial velocity	κ	$[-]$	isentropic exponent
l	$[m]$	length of wires	$\dot{M}$	$[\frac{kg}{h}]$	mass flow
$\dot{m}$	$[\frac{kg}{m^2 \cdot s}]$	mass flow density	$m_r(\bar{\alpha})$	$[-]$	central moment of order r of the distribution of α
p	$[Pa]$	pressure	R_i	$[\Omega]$	resistance of area i
T	$[K]$	temperature	t	$[s]$	time
v	$[\frac{m}{s}]$	velocity	W	$[J]$	energy
$\dot{x}$	[-]	gas mass flow fraction			

Greek Symbols

$\dot{\alpha}$	[-]	gas fraction of volumetric flux	α	[-]	void fraction
λ	$[m]$	Laplace length	ρ	$[\frac{kg}{m^3}]$	density
σ	$[\frac{N}{m}]$	surface tension			

Indices

0	upstream the nozzle	1	inside the nozzle
2	after acceleration to critical velocity and before the expansion	3	in the spray
∞	far away from the nozzle	$2ph$	two-phase
c	critical	D	smallest cross section of the nozzle
g	gas	i	index of area between two wires
l	liquid	M	measured in the direction M

1. Introduction

A spray of small droplets is formed by the atomization of a liquid or a suspension in two-phase atomizers. The mean goal is either a narrow distribution of the droplet diameter or the generation of large phase interfaces of the liquid in order to increase the heat- and mass-transfer in the spray.

In two-phase gas-liquid atomizers the pressurized gas phase is dispersed within the liquid phase. The two-phase mixture is accelerated within a cone. In the narrowest cross section critical mass flow is observed. Leaving the nozzle the gas flow expands and the liquid is dispersed into ligaments. The ligaments decompose into droplets. The spatial and the time distributions of the mean droplet diameters and the droplet velocities inside the spray depend on the total pressure in front of the nozzle, the volumetric flow rate of liquid and gas, as well as on the spatial and time distribution of gas and liquid at the exit orifice. These distributions are effected by the construction of the gas inlet into the mixing chamber and by the two-phase flow inside the mixing chamber and the nozzle. Several studies on this so called effervescent atomizers have been conducted by the groups of Lefebvre [2, 3, 5, 6, 19, 20, 23] and Sojka [4, 1, 11, 12, 13, 14, 15, 22, 25]. Some publications are listed in tabulars 1 and 2.

The paper of Chin and Lefebvre [6] is the only one which takes the flow regime inside the atomizer into account. The flow regime is visualized by high speed images. Then curves for duty points are added to the flow map of Oshinowo and Charles fig. 1 for vertical downward operating atomizers. Curves for duty points of horizontal operating atomizers are also added to the flow map of Baker. Chin and Lefebvre vary the total pressure at the entrance of the atomizer, the viscosity and the surface tension. They discuss the influence of those parameters on the flow regime but do not compare the results to the high speed images. Within this work duty points of the mixing chamber and the nozzle of the atomizer used here are additionally added to the map fig. 1.

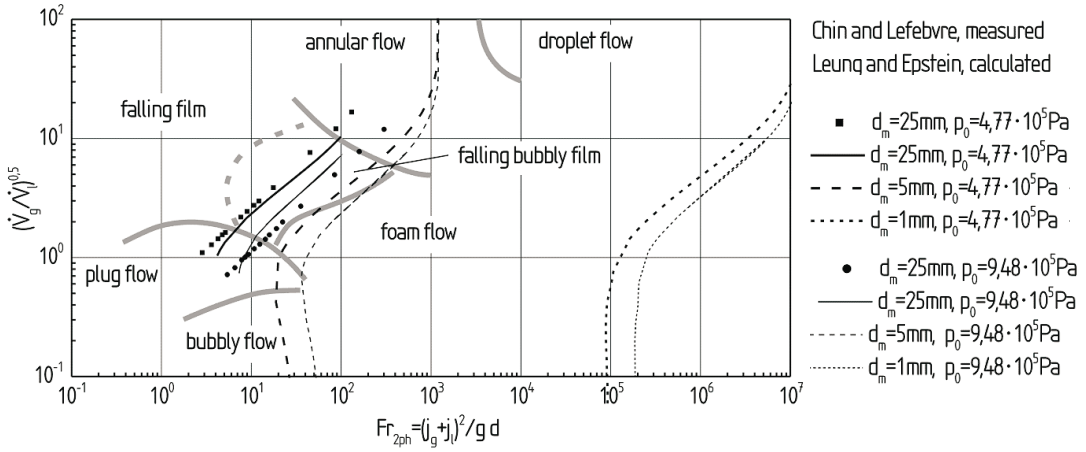

Fig. 1: Flow map of Oshinowo and Charles containing mesurements of Chin and Lefebvre [6], own calculations for the mixing chamber with a diameter of 25mm used from Chin and Lefebvre and of 5mm used in our own test facility. In Addition calculations for the nozzle with a diameter of 1mm are depicted.

It can be seen that the flow map does not predict the flow regime inside the nozzle. For the flow regime inside the mixing chamber the flow map seems to give the wrong answer because it is only valid for fully developed velocity fields. Here this is not the case due to the short flow length inside the atomizer.

author	liquid/gas	$\dot{x}[-]$	$p_{abs}[Pa]$	$\sigma[N/m]$	$\eta[Pa \cdot s]$	d_D[mm]	$\dot{M}[kg/h]$
Wallis, Sullivan [1]	water/air		$1.1 - 3.8 \cdot 10^5$	0.072	0.001	5 constructions	$54 - 97.2$
Lefebvre, Wang, Martin [2]	water/nitrogen	$0.002 - 0.022$	$1.34 - 7.9 \cdot 10^5$	0.072	0.001	$0.8 - 2.4$	
Lund, Sojka, Lefebvre, Gosselin [3]	water, water-glycerin, siliconoil/air	$0.01 - 0.065$	$2.39 - 5.15 \cdot 10^5$	$0.030 - 0.072$	$0.001 - 0.080$		≤ 5.4
Lund, Jian, Sojka, Gore, Panchagnula [4]	oil/helium, methan, propan	$0.048 - 0.333$	$2.39 - 5.15 \cdot 10^5$	0.030	0.005		≤ 1.8
Whitlow, Lefebvre [5]	water/nitrogen	$0.005 - 0.038$	$1.7 - 7.9 \cdot 10^5$	0.072	0.001	$0.8 - 2.4$	$6.8 - 335$
Chin, Lefebvre [6]		$0.006 - 0.375$	$1.73 - 8.48 \cdot 10^5$	$0.024 - 0.073$	$0.001 - 0.125$	4.14	460
Buckner, Sojka [7]	glycerin-water/air	$0.048 - 0.260$	$2.1 - 3.3 \cdot 10^5$		0.4		$36 - 252$
Chawla [8, 9]	wastewater, acids etc. /air	$0.09 - 0.17$	$6 \cdot 10^5$			$2.0 - 12.0$	
Chawla [10]	water/air	$0.0009 - 0.6$	$1.5 - 5 \cdot 10^5$	0.072	0.001		$10 - 225$
Bush, Sojka [11]	water/air	$0.01 - 0.056$					$3, .6$
Sutherland, Sojka, Plesniak [12]	siliconoil, water-glycerin/air	$0.005 - 0.038$	$5.4 - 7.5 \cdot 10^5$	$0.030 - 0.072$	$0.02 - 0.08$	porous plates	$1.8 - 3.6$
Wade, Weerts, Sojka, Gore, Eckerle [13]	synth. fuel/nitrogen	$0.048 - 0.23$	$120 - 330 \cdot 10^5$		0.0028	$0.18 - 0.34$	
Sovani, Crofts, Gore, Sojka, Eckerle [14]	synth. fuel/nitrogen	$0 - 0.078$	$124 - 289 \cdot 10^5$			0.25	discontinuous
Sovani, Sojka, Gore, Crofts, Eckerle [15]	synth. fuel/nitrogen	$0.001 - 0.2$	$35 - 315 \cdot 10^5$			$0.18 - 0.35$	discontinuous
Jang, Choi [16]	testfuel/nitrogen		$10 - 70$				discontinuous
Landwehr, Schmidt, Walzel [17]	water/air	$0.0004 - 0.078$	$1.3 - 2.6 \cdot 10^5$	0.072	0.001	$10mm$	$400 - 1500$
Sher, Koren, Katoshevski,Kholmer [18]	water/air	$0.17 - 0.29$	$3 - 4 \cdot 10^5$	0.072	0.001	1	
Chen, Lefebvre [19]	syrup-water/air	$0.015 - 0.260$	$2.36 - 10 \cdot 10^5$	$0.030 - 0.082$	$0.001 - 0.1$	$1.2 - 2.0$	$36 - 252$
Chen, Lefebvre [20]	water, syrup-water, siliconoil/air	$0 - 0.107$	$1.41 - 2.3 \cdot 10^5$	$0.030 - 0.080$	$0.001 - 0.023$	1.6	
Raetzo [21]	water/air	$0.123 - 0.574$	$4.1 - 7.8 \cdot 10^5$	0.072	0.001	18	$345 - 1157$
Luong, Sojka [22]	siliconoil, water-glycerin/air	$0.015 - 0.065$		$0.033 - 0.065$	$0.03 - 0.124$		$2.2 - 3.6$
Roesler, Lefebvre [23, 24]	water/air	$0.001 - 0.048$	$1.73 - 6.9 \cdot 10^5$	0.072	0.001	$0.8 - 2.0$	
Panchagnula, Sojka [25]	syrup-water/air	$0.02 - 0.09$		0.067	0.900	$3.0 - 4.5$	$108 - 432$
Lörcher [26]	water/air	$0.003 - 1$	$3 - 15 \cdot 10^5$	0.072	0.001	$0.5 - 2.0$	$2 - 100$

Table 1: Experimental investigations on effervescent atomizers

author	measurement technique	droplet size	varied parameter	investigated parameter
Wallis, Sullivan [1]			p_0	$\dot{M}_l$, $\dot{M}_g$
Lefebvre, Wang, Martin [2]	laser diffraction particle size analyser	$20\mu m < d_{32} < 300\mu m$	p_0, $\dot{x}$, d_D	d_{32}, RRSB-parameter
Lund, Sojka, Lefebvre, Gosselin [3]	laser diffraction particle size analyser	$40\mu m < d_{32} < 60\mu m$	p_0, $\dot{x}$, η, σ	d_{32}
Lund, Jian, Sojka, Gore, Panchagnula [4]	laser diffraction particle size analyser	$30\mu m < d_{32} < 80\mu m$	molar mass of gas	d_{32}, RRSB-parameter,v_d
Whitlow, Lefebvre [5]	laser diffraction particle size analyser	$20\mu m < d_{32} < 70\mu m$	p_0, $\dot{x}$, x	probabilitydensityf. for d_d, RRSB-parameter, mass flow distribution
Chin, Lefebvre [6]		p_0, $\dot{x}$, η, σ	Flow regime inside the mixing chamber	
Buckner, Sojka [7]	laser diffraction, high speed ph.	$15\mu m < d_{32} < 50\mu m$	p_0, $\dot{x}$, η	d_{32}
Chawla [8, 9]	PDA		x	probability density functions for d_d und v_d
Chawla [10]		$30\mu m < d_{32} < 100\mu m$	$\dot{M}_l$, $\dot{M}_g$	d_{32}
Bush, Sojka [11]		$30\mu m < d_{32} < 70\mu m$	$\dot{x}$, x	d_{32}, $\dot{M}_e$
Sutherland, Sojka, Plesniak [12]	laser diffraction particle size analyser high speed photography	$60\mu m < d_{32} < 230\mu m$	p_0, $\dot{x}$, σ	d_{32}
Wade, Weerts, Sojka, Gore, Eckerle [13]	laser diffraction particle size analyser		p_0, $\dot{x}$, d_D, r	d_{32}, RRSB-parameter, sprayangle
Sovani, Crofts, Gore, Sojka, Eckerle [14]	high speed photography		p_0, $\dot{x}$, needlelift	sprayangle, mass flow, penetration depth
Sovani, Sojka, Gore, Crofts, Eckerle [15]	laser diffraction particle size analyser high speed photography	$3\mu m < d_{32} < 10\mu m$	p_∞, p_0, d_D	d_{32}, Häufigkeitsdichteverteilungen, flow regime inside the mixing chamber
Jang, Choi [16]	high speed ph., opt. patternator	$d_{32} < 70\mu m$	p_∞, p_0, construction	mass flow distribution, sprtial resolution of d_{32}
Landwehr, Schmidt, Walzel [17]	mech. probe with one chanel		p_∞, p_0, $\dot{x}$, r	mass flow distribution, p_2, c, $\dot{M}$
Sher, Koren, Katoshevski,Kholmer [18]	laser diffraction particle size analyser	$4\mu m < d_{32} < 30\mu m$	p_0, $\dot{x}$, construction	d_{32}
Chen, Lefebvre [19]	high speed ph.		p_0, p_∞, $\dot{x}$, η, σ, d_D	$\dot{M}_e$
Chen, Lefebvre [20]			p_0, p_∞, $\dot{x}$, η, σ	spray angle, $(p_2/p_\infty)_c$
Raetzo [21]	mech. Patternator, PDA	$50\mu m < d_{32} < 90\mu m$	p_0, $\dot{x}$	mass flow distribution, d_d, v_d, $\dot{M}_e$
Luong, Sojka [22]	PDA	$d_{min} = 3\mu m$, $d_{max} = 60\mu m$	p_0, $\dot{x}$, η, σ, x, r	time distance between two dopplerbursts
Roesler, Lefebvre [23, 24]	laser diffraction particle size analyser	$30\mu m < d_{32} < 120$	p_0, x	d_{32}, RRSB-parameter
Panchagnula, Sojka [25]	PDA	$60\mu m < d_{32} < 90$	$\dot{M}$, $\dot{x}$, x, r	number averaged droplet velocity, d_{32}
Lörcher [26]	PDA	$20\mu m < d_{32} < 100$	p_0, $\dot{x}$, x, r, d_D, construction	probability density function for d_d and v_d d_{32}, d_{10}, $\bar{v}_d$ flow regime inside mixing chamber and nozzle

Table 2: Experimental investigations on effervescent atomizers

Therefore this project was established to predict the phase distribution at the exit cross section of the atomizer and to describe the influence of this phase distribution on the characteristics of the resulting spray. To show the interaction between gas and liquid at the exit orifice fig. 2 was taken. An undisturbed liquid jet leaves the nozzle and one bubble is accelerated inside the conical part of the atomizer. When the bubble reaches the exit orifice the jet expands and is immediately disintegrated. The number of generated ligaments is high enough to absorb all the light. The spray appears black.

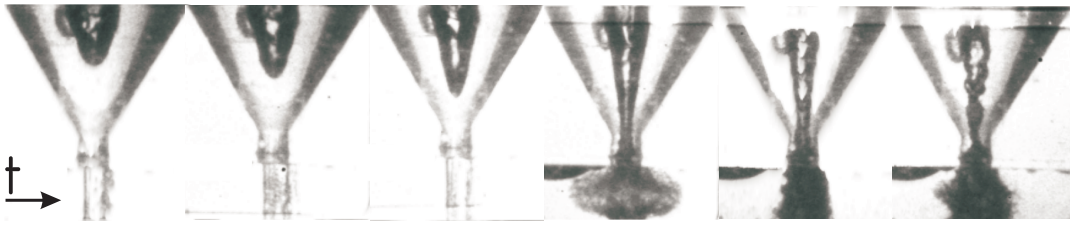

Fig. 2: Disintegration of the liquid with and without gas for identical pressure and liquid flow rate at the exit of the nozzle, exposure time of each picture $1\mu s$, time between pictures $100\mu s$, $p_0 = 6 \cdot 10^5 Pa$, $\dot{x} < 1 \cdot 10^{-3}$

2. Experimental Apparatus

In the present work the experiments are performed with an atomizer in which gas and liquid are premixed inside a mixing chamber upstream the nozzle. The total pressure in front of the nozzle is varied in different experiments $(p_0 < 1.6MPa)$. The investigated atomizer is presented in fig. 3. Temperature, pressure and mass flow of both phases are measured at the

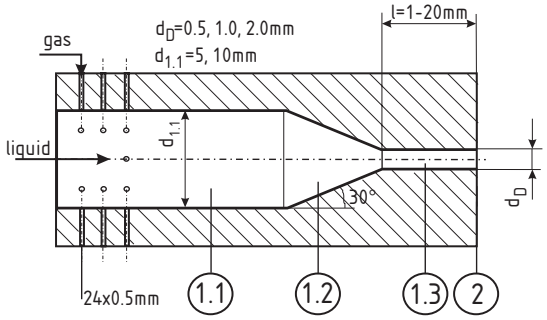

Fig. 3: Schematic diagram of the atomizer: 1.1 mixing chamber, 1.2 conical part, 1.3 nozzle, 2 exit cross section

entrance of the atomizer . The flow regime inside the mixing chamber is visualized by means of a high speed camera. The radial profile of the void fraction inside the nozzle is measured with an electrical tomographic measurement technique by Lörcher, Schmitz and Mewes [27]. The axial profile of the void fraction is measured by a similar measurement technique. To identify the different flow regimes a statistical analysis of the axial profiles is done. The flow regimes are analyzed for different pressures and designs of the gas dispenser.

3. Void fraction inside the mixing chamber

Different flow regimes are recognized in the mixing chamber by detecting single short plugs and bubbles covering the whole cross section. In the axial direction wires are placed inside

the nozzle at a distance of 2 mm to each other. The conductance between a pair of wires is measured with frequencies of about 4000 Hz.

The measured conductance is respectively a function of the distribution of the liquid and the gas flow between two wires. Depending on the flow pattern the wires are proportionate electrically connected by liquid. This corresponds to a parallel arrangement of electrical resistors.

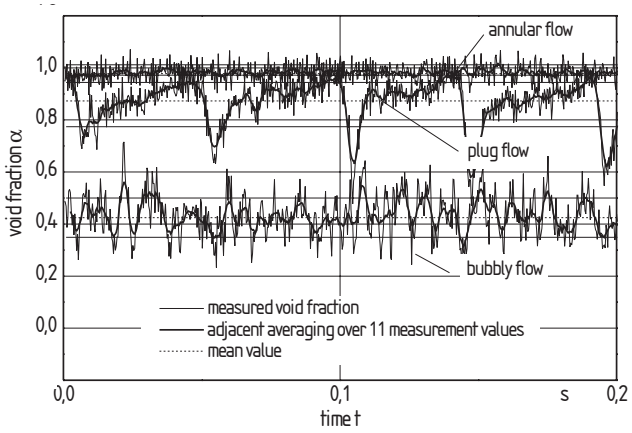

Fig. 4: Measured void fraction between two wires for bubbly flow, plug flow and annular flow as a function of time

The measured void fraction is shown for one pair of wires in fig. 4. For bubbly flow the void fraction is relatively low and oscillates with a high amplitude around the mean value. Plug flow is characterized by a short period of a low void fraction followed by a long period of a constant high void fraction. For annular flow the void fraction is close to one and the oscillation around the mean value is small. In fig. 4 the different flow regimes are easy to distinguish, but especially in the transient regions between two flow regimes, the classification might be user-dependent. That is why a statistical criterion has to be introduced to analyze the current flow regime from the measured axial profile of the void fraction.

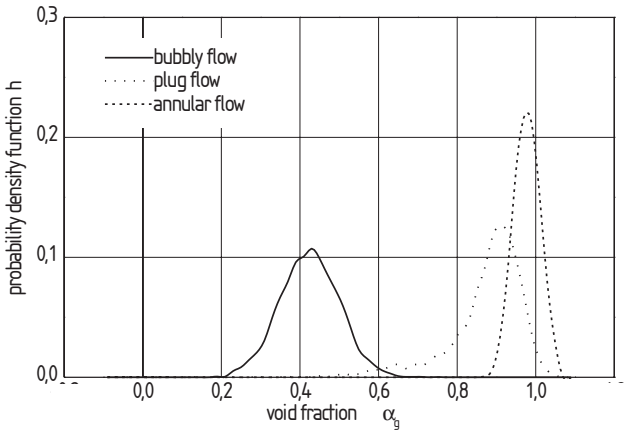

Fig. 5: Probabiltity density function for bubbly flow, plug flow and annular flow as a function of the void fraction

Therefore the probability density function is presented in fig. 5 as a function of the void fraction with the data from the three experiments shown in fig. 4. For bubbly flow the probability density function is symmetric and the distribution is wide ranged. The distribution for plug

flow is not symmetric. The short plugs occur not very often and have a low probability. Thus the distribution is asymmetric. For annular flow the distribution is symmetric again and very narrow ranged.

In statistics the expression for the asymmetry g is defined by the ratio of the third and the second central moment of the distribution with

$$g \equiv \frac{m_3(\bar{\alpha})}{\underset{n}{m_2}(\bar{\alpha})^{3/2}} \tag{1}$$

$$g \equiv \frac{\frac{1}{n}\sum_{i=1}(\alpha_i - \bar{\alpha})^3}{\left[\frac{1}{n}\sum_{i=1}^{n}(\alpha_i - \bar{\alpha})^2\right]^{3/2}}. \tag{2}$$

In eqn. (1) and (2) $\bar{\alpha}$ is the mean value of all measured void fractions and α_i is the i^{th} void fraction of one experiment. This expression for the asymmetry is calculated for several experiments performed at different total pressures upstream the nozzle and different gas mass flow fractions. In fig. 6 the asymmetry is shown as a function of the energy ratio.

The energy ratio e is defined by the ratio of the isothermic compression energy needed to pressurize the gas mass flow rate from atmospheric pressure to the total pressure in front of the nozzle and the potential energy of the supplied liquid mass flow rate

$$e = \frac{\dot{M}_g \frac{p_\infty}{\rho_{g,\infty}} ln(\frac{p_0}{p_\infty})}{\dot{M}_l \frac{p_0 - p_\infty}{\rho_l}} . \tag{3}$$

The mass flow rates of gas and liquid can be written as

$$\dot{M}_g = \dot{m}_c \cdot A_D \cdot \dot{x} \tag{4}$$

$$\dot{M}_l = \dot{m}_c \cdot A_D \cdot (1 - \dot{x}) . \tag{5}$$

$\dot{m}_c$ is the critical mass flow density and A_D is the cross section of the exit orifice. Using the expressions for the mass flow rates of gas and liquid eq. (3) can be transformed into

$$e = \frac{\dot{x}}{(1-\dot{x})} \frac{p_\infty}{p_0 - p_\infty} \frac{\rho_l}{\rho_{g,\infty}} ln\left[\frac{p_0}{p_\infty}\right] . \tag{6}$$

The energy ratio depends on the gas mass flow fraction $\dot{x}$ and the total pressure in front of the nozzle p_0.

For low energy ratios the asymmetry is about zero, the distribution of the frequency of occurrence is symmetric. For higher energy ratios the asymmetry becomes negative and the distribution leans toward higher energy ratios. If the energy ratio is increased further the asymmetry becomes about zero again. The high energy ratios are calculated for annular flow. The measured values are approximated by the curve shown in fig. 6. The three different flow regimes are each represented by a horizontal line. Between the explicit flow regimes transition regions are found. The values of the energy ratio at the end of the horizontal lines are taken to define the transition regions in the new Ohnesorge diagram suggested at the end of this paper. The measurement of the void fraction and the calculation of the asymmetry from the measured void

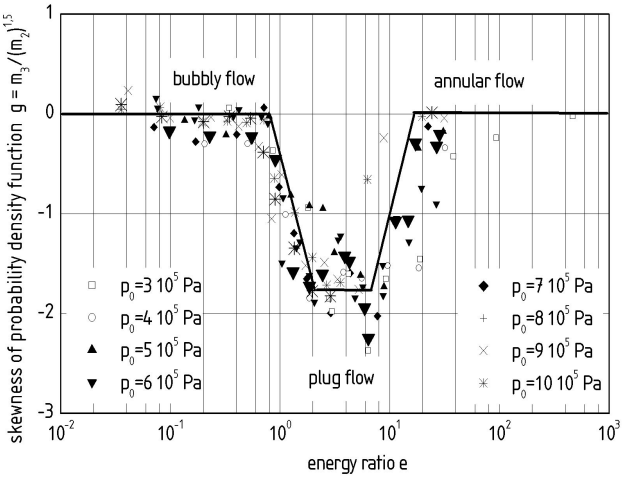

Fig. 6: Asymmetry of the distribution of the void fraction as a function of the energy ratio for different pressures

fraction are reproduceable and user independent. Thus a criterion has been found to describe the transition between the different flow regimes inside the mixing chamber of the atomizer.

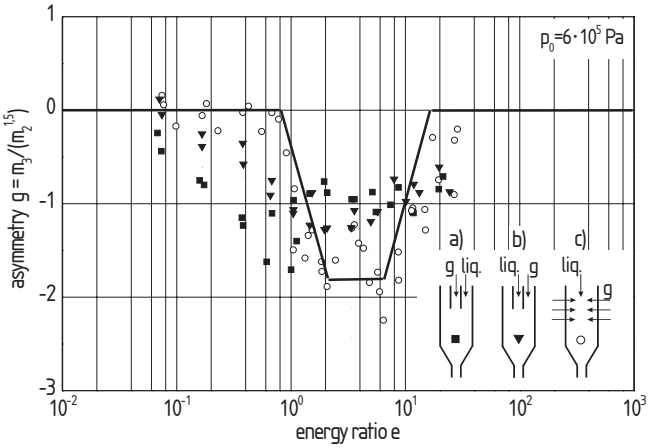

Fig. 7: Asymmetry oft the distribution of the void fraction as a function of the energy ratio for different gas dispersers inside the atomizer

In fig. 7 the asymmetry is again presented as a function of the energy ratio. Here the design of the gas disperser is varied. Form the results it can be seen that the design has a significant influence on the flow regime. This was already expected because of the very short flow length and the not fully developed velocity field.

Constant spray conditions were found for bubbly flow and annular flow. To operate the atomizer with those two flow regimes and achieve an asymmetry near zero different designs of the gas disperser have to be used.

4. Void fraction inside the nozzle

After passing the cylindrical part of the mixing chamber the cross section of the flow is reduced and the two-phase mixture is accelerated. Therefore the pressure decreases and the gas phase expands. The bubble size increases and for higher ratios of the orifice length to the orifice diameter l/d the bubbles are divided into many smaller ones. The observations are performed

with a high speed camera using an extreme short exposure time (fig. 8).

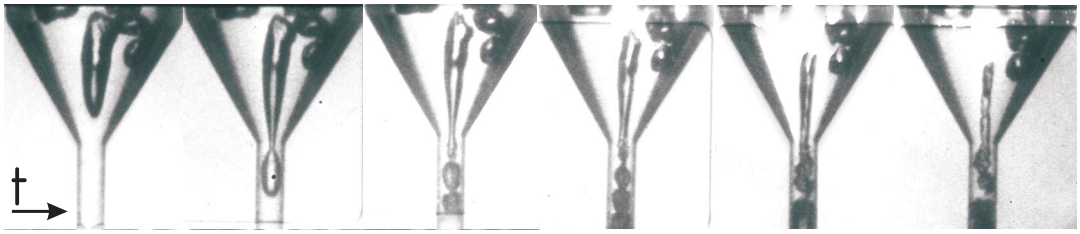

Fig. 8: Expansion and dissipation of single bubbles in the conical part of the atomizer and the exit cross section, exposure time $1\mu s$, time between pictures $100\mu s$, $p_0 = 6 \cdot 10^5 Pa$, $\dot{x} < 1 \cdot 10^{-3}$

The diameter of the cylindrical orifice itself is varied between 0.5 and $2.0mm$. In case of diameters in the range of $0,1\lambda - 1,0\lambda$ with $\lambda = \sqrt{\sigma/g(\rho_l - \rho_g)}$ representing the Laplace length scale, the surface forces overcome the lift forces. In this case the flow channel is called microchannel. In microchannels the flow regimes occur in a different manner and can not be described by the energy ration. To detect the flow regime inside the nozzle a sensor with two photoelectric relays located near to the exit cross section was designed (fig. 9).

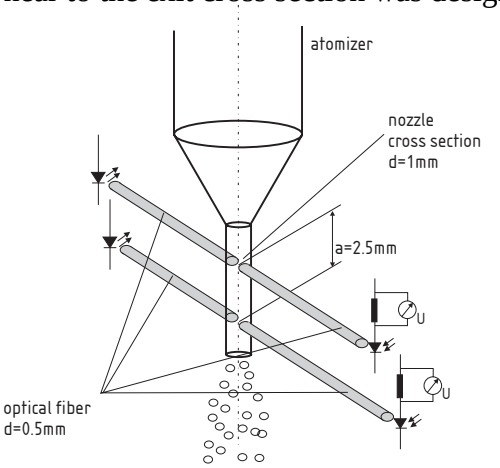

Fig. 9: Optical sensor with two photoelectric relays located at the exit cross section to measure the phase distribution and the velocity inside the nozzle.

A red laser diodes light is fed in an optical fiber. The end of this fiber faces the microchannel. The laser beam crosses the channel and the transmitted light is detected by a photo diode via a second fiber optic. The deviation of the voltage is shown in fig. 10 for homogeneous bubbly flow and for plug flow. The time dependency of this signal is significant for the different flow regimes. With this measurement technique also the flow regime inside the microchannel close to the exit orifice can be detected. By comparing the signals from the two photoelectric relays the velocities of the plugs can be calculated.

The visualized phase distributions and the measured velocities are compared with the results of a numerically calculated flow field. Therefore a grid was generated which is presented in fig. 11. Some phase distributions are shown as a function of the time in fig. 12. Compared to the high speed images the bubble is stretched and becomes very thin at the transition from the conical section to the cylindrical exit cross section.

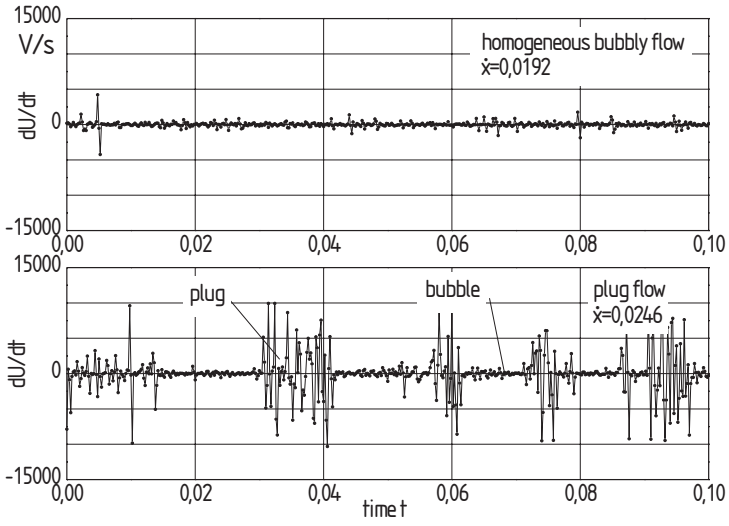

Fig. 10: Deviation of the voltage as a function of time for two flow regimes

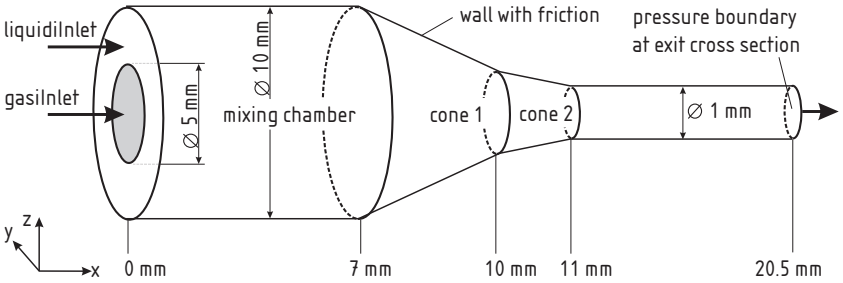

Fig. 11: Grid for the numerical calculation of the flow field, 36075 knots, 189454 tetrahedrons, time step width $1 \cdot 10^{-4} s$, calculated flow time $1.35 \cdot 10^{-}2s$

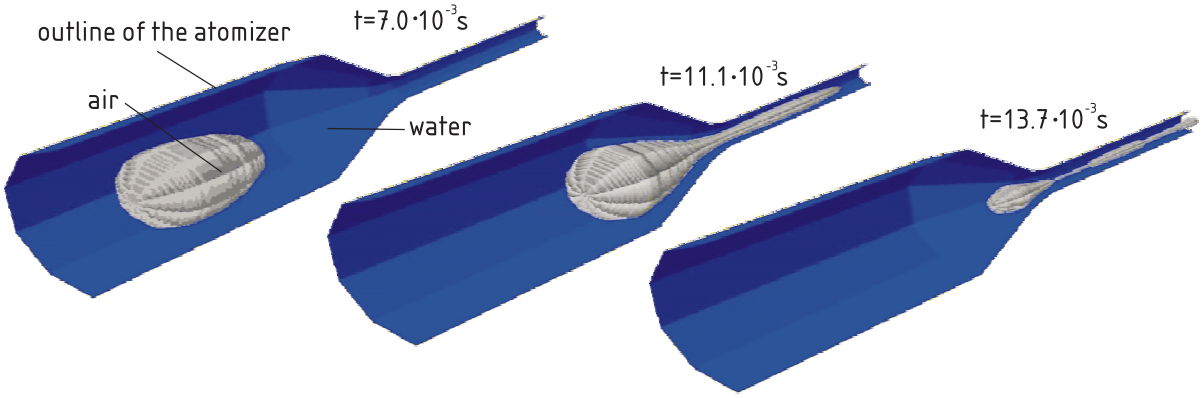

Fig. 12: Phase distribution inside the atomizer as a function of the time, $p_0 = 6 \cdot 10^5 Pa$, $v_{g,0} = 1,.0m/s$, $v_{l,0} = 1.0m/s$

5. Conclusions

Atomizing two-phase gas-liquid flows, the spatial and the time distribution of the mean droplet diameter inside the spray depend not only on the total pressure in front of the nozzle, but also on the volumetric flow rate of liquid and gas and the flow regime inside the nozzle.

An electrical measurement technique is presented for the axial profile of the void fraction with a high time resolution. The different flow regimes can be identified by a statistical analysis of the measured axial profile of the void fraction. The flow regimes depends on the energy ratio. It is defined by the ratio of the isothermic compression energy needed to pressurize the gas mass flow rate from atmospheric pressure to the total pressure in front of the nozzle and the potential energy of the supplied liquid mass flow rate.

Different models for calculating the critical mass flow rate are presented and compared to experimental results.

Acknoledgement

The authors wish to thank the German Research Foundation (DFG) for their financial support.

REFERENCES

[1] G. B. Wallis, D. A. Sullivan: Two-phase air-water nozzle flow; *Journal of Basic Engineering*, **94** (1972) 4, 788-794

[2] A.H. Lefebvre, X.F. Wang, C.A. Martin: Spray characteristics of aerated-liquid pressure atomizers; *J. Propulsion*, **4** (1988) 4, 293-298

[3] M. T. Lund, P. E. Sojka, A. H. Lefebvre, P. G. Gosselin:Effervescent atomization at low mass flow rates. Part 1: The influence of surface tension; *Atomization and Sprays*, **3** (1993),77-89

[4] M.T. Lund, C.Q. Jian, P.E. Sojka, J.P. Gore, M.V. Panchagnula: The influence of atomizing gas molecular weight an low mass flowrate effervescent atomizer performance; *FED-Vol.178/ HTD-Vol. 270, Fluid Mechanics and Heat Transfer in Sprays, ASME*(1993) 123-128

[5] J.D. Whitlow, A.H. Lefebvre: Effervescent atomizer operationand spray characteristics; *Atomization and Sprays*, **3** (1993),137-155

[6] J. S. Chin, A. H. Lefebvre: Flow patterns in internal-mixing, twin-fluid atomizers; *Atomization and Sprays*, **3** (1993), 463-475

[7] H.N. Buckner, P.E. Sojka: Effervescent atomization of high-viscosity fluids: Part I: Newtonian liquids; *Atomization and Sprays*, **1** (1991), 239-252

[8] J.M. Chawla: Flüssigkeitsinhalt in Rohren für Flüssigkeits/Gas-Gemische bei der Zweiphasenströmung; *Chem.-Ing.-Tech.*, **5+6** (1969), 328-330

[9] J. M. Chawla: Effect of the droplet agglomeration on the design of spray dryer towers; *Drying Technology* **12** (1994) 6, 1357-1365

[10] J. M. Chawla: Der Naßabscheider CWS; *Chemie-Technik* **8** (1979) 10, 511-513

[11] S.G. Bush, P.E. Sojka: Entrainment by effervescent sprays at low mass flow rates; *FED-Vol. 178/HTD-Vol.270, Fluid Mechanics and Heat Transfer in Sprays*, ASME, USA (1993) 117-121

[12] J. J. Sutherland, P. E. Sojka, M. W. Plesniak: Ligament-controlled effervescent atomization; *Atomization and Sprays* **7** (1997) 383-406

[13] R. A. Wade, J. M. Weerts, P. E. Sojka, J. P. Gore, W. A. Eckerle: Effervescent atomization at injection pressures in the MPa Range; *Atomization and Sprays* 9 (1999) 651-667

[14] S. D. Sovani, E. Chou, P. E. Sojka, J. P. Gore, W. A. Eckerle, J. D. Crofts: Cone angles for effervescent atomizers spraying into high pressure environments; *Proceedings of the Central States Section / Combustion Institute, 1998 Technical Meeting*,Lexington KY, USA (1998)

[15] S. D. Sovani, P. E. Sojka, J. P. Gore, J. D. Crofts, W. A. Eckerle: Effervescent diesel injection: Injector internal flow and its influence on spray quality; *ICLASS 2000*, Pasadena, USA (2000)

[16] C. Jang, S. Choi: Comparison of the overall performance between an air-assisted fuel injector and a high-pressure swirl injector; *ICLASS 2000*, Pasadena, USA (2000)

[17] F. Landwehr, D. Schmidt, P. Walzel: Messung und Berechnung des kritischen Druckverhältnisses an Zweistoff-Düsen; *Spray '99*, Germany (1999)

[18] E. Sher, M. Koren, D. Katoshevski, V. Kholmer: Energy consideration and experimental study of effervescent atomizers; *ILASS-Europe 2000*, Darmstadt, Germany (2000)

[19] S.K. Chen, A.H. Lefebvre: Discharge coefficients for plain-orifice effervescent atomizers; *Atomization and Sprays*, **4** (1994) 275-290

[20] S.K. Chen, A.H. Lefebvre: Spray cone angles of effervescent atomizers; *Atomization and Sprays*, **4** (1994) 291-301

[21] T. Raetzo: Charakterisierung von Düsen zum Zerstäuben von Flüssigkeiten; Dissertation, ETH Zürich (1995)

[22] J.T.K. Luong, P.E. Sojka: Unsteadiness in effervescent sprays; *Atomization in Sprays*, **9** (1999) 87-109

[23] T.C. Roesler, A.H. Lefebvre: Studies on aerated-liquid atomization; *Int. J. Turbo and Jet Engines*, **6** (1989) 221-230

[24] T.C. Roesler: An experimental study of aerated-liquid atomization; Ph.D. Thesis, Purdue University, West Lafayette, IN (1988)

[25] M. V. Panchagnula, P. E. Sojka: Spatial droplet velocity and size profiles in effervescent atomizer-produced sprays; *Fuel* (1999) **78**, 729-741

[26] M. Lörcher: Zerstäuben von zweiphasigen Gemischen aus Flüssigkeiten und Gasen; *VDI Fortschritt-Berichte*, Reihe 3, 764, VDI Verlag, Düsseldorf, ISBN 3-18-376403-2 (2003)

[27] M. Lörcher, D. Schmitz, D. Mewes: Tomographic measurement techniques - Visualization of multiphase flows; *Machine Graphics & Vision* , **8** (1999) 4, 667-679

[28] E. B. Wylie , V. L. Steeter: Fluid transients; FEB Press, Michigan USA (1982) ISBN 0-9619144-0-7

[29] M. Chawla, P. v. Böckh: Kritische Massenstromdichte von Flüssigkeits / Gas-Gemischen; *Chem.-Ing.-Techn.*, **43** (1971) 20, 1106-1108

[30] J.C. Leung, M. Epstein: A generalized correlation for two-phase nonflashing homohenous choked flow; Transactions of the ASME, *Journal of Heat Transfer* (1990) **112**, 528-530

[31] R. Mauri, G. P. Beretta: A simplified model of two-phase flow in nozzles; Proc. of the 2nd ASME-JSME Thermal Engineering Joint Conf., Honolulu, HI, USA (1987)

[32] H. J. Richter: Seperated two-phase flow model, application to critical two-phase flow; *Int. J. Multiphase Flow*, **9** (1983) 5, 511-530

[33] R. F. Tangren, C. H. Dodge, H. S. Seifert: Compressibility effects in two-phase flow; *J. of Applied Physics*, (1949) **20**, 637-645

[34] S. W. Churchill, R. Usagi: A general expression for the correlation of rates of transfer and other phenomena; *AIChE Journal*, **18** (1972) 6, 1121-1128